Localization of Autonomous Underwater Vehicles using Airborne Visible Light Communication Links

Jaeed Bin Saif, Mohamed Younis, Fow-Sen Choa Department of Computer Science and Electrical Engineering University of Maryland Baltimore County Baltimore, Maryland, USA jaeedb1, younis, choa@umbc.edu Akram Ahmed
Computer Engineering Department
King Fahd University of Petroleum and Minerals
Dhahran, Saudi Arabia
akram@kfupm.edu.sa

Abstract—In an application involving Autonomous Underwater Vehicles (AUV) it is important to track the trajectory and spatially correlate the collected data. Relying on an Inertial Navigation System (INS) while factoring in the initial AUV position would not suffice given the major accumulated errors. Employing surface nodes is a logistically complicated option, especially for missions involving emerging events. This paper proposes a novel localization approach that offers both agility and accuracy. The idea is to exploit a communication mechanism across the air-water interface. In particular, we employ an airborne unit, e.g., a drone, that scans the area of interest and uses visual light communication (VLC) to reach the AUV. In essence, the airborne unit defines virtual anchors with known GPS coordinates. The AUV uses the light intensity of the received VLC transmissions to estimate the range relative to the anchor points and then determine its own global coordinates at various time instances. The proposed approach is validated through extensive simulation experiments. The simulation results demonstrate the viability of our approach and analyze the effect of the VLC parameters.

Keywords— Underwater localization; Visible light communication, AUV tracking, air-to-water communication.

I. INTRODUCTION

Advances in underwater sensing solutions have been mainly driven by the interest in applications like marine biology, pollution control, tsunami prediction, search and rescue, and security surveillance [1]. Existing solutions can be categorized based on the employed nodes into stationary and mobile. The former is geared for long missions where nodes are anchored to rocks or to the seabed. The second category suits emerging events or sessional short missions where one or multiple AUVs are deployed to collect data or track a phenomenon or object. For the data to be useful it has to be correlated to the context, both temporally and spatially. Spatial correlation can be based on either landmarks or a coordinate system. Proximity to landmarks is often of little value given the vast area to be covered by a mission and due to the fact that these landmarks themselves should be pre-mapped. The use of a coordinate system is deemed the most effective option.

Establishing a global coordinate system, such as GPS, underwater is quite challenging. The main issue is the lack of reference anchors that are reachable throughout the world, add to that the scale as water covers 70% of the earth's surface. The conventional method to mitigate such a challenge is to deploy surface nodes, e.g., buoys, or boats; these surface nodes will have a GPS receiver to know their position and broadcast beacons that underwater nodes can use for ranging and multilateration [2]. However, such a method has serious

shortcomings. First, it lacks flexibility and responsiveness since deploying the boats or buoys takes a long time, especially for distant areas; for an emerging event, it is necessary to rapidly get AUVs to operate. Second, for applications like security surveillance and combat reconnaissance, the presence of surface nodes is deemed to be risky and highly undesirable. For the same reason, an AUV should not move to the surface to use GPS signals to calibrate its position tracking. Therefore, an alternative approach is needed for localizing mobile underwater nodes.

This paper opts to fill the technical gap by proposing a novel localization approach that suits dynamic underwater sensing missions. First, we point out that GPS signals do not reach underwater since radio waves suffer very high attenuation in water due to its high absorption coefficient. Since the use of a surface node is to be avoided, the GPS coordinates need to be shared through cross-medium communication. For that VLC is a prime candidate [3]. VLC provides substantially more bandwidth than the other modes of communication without the need for any gateway node [4][5]. Recent studies have also characterized the behavior of the VLC in the air-to-water medium [6] and devised proper modulation and encoding schemes to ensure high bit rate and low bit error rate[7][8]. This paper leverages these studies and devises a novel protocol for global AUV localization using an airborne unit (GAULA).

GAULA, which means yell, strives to introduce virtual anchors with known GPS coordinates for localizing AUV. In GAULA, an airborne node is deployed to scan the area of interest, i.e., where an AUV operates. The airborne node (AN), which can be a drone, directs VLC transmissions with encoded global coordinates and additional information in order to aid the AUV in estimating its position. The area is mapped to a grid where the AN targets the center of each cell with a modulated light beam, as illustrated in Fig. 1. The transmission power is set such that the cell is fully covered at a certain underwater depth. The AUV uses its depth and the sensed light intensity from an airborne transmission to estimate its proximity to the cell center. By receiving multiple transmissions at different cells, the AUV projects the various ranges to the same x-y plane (same underwater depth) and factors in its trajectory to determine its global coordinates. The performance of GAULA is validated through simulation. The simulation results confirm GAULA's effectiveness of in achieving accurate positioning under varying transmission parameters and AUV movement patterns.

This paper is organized as follows. GAULA is set apart from existing work in Section II. Section III covers the system model

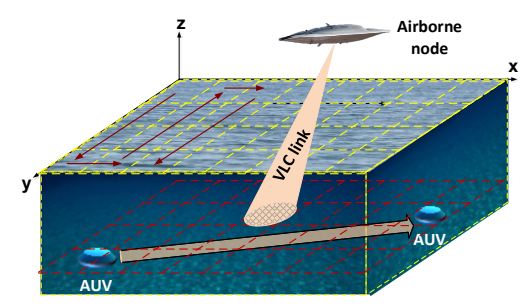


Fig. 1: GAULA maps the area as a grid that is scanned by the AN in a specific order. Each cell on the grid is targeted by a VLC transmission reflecting the cell GPS coordinates. The AUV receives transmission at different light intensity depending on its location within the cell and its depth. By receiving multiple transmissions (at different cells), the AUV can calculate its global coordinates

and discusses VLC-ranging based on the light intensity. Section IV describes GAULA in detail. Section V shows the simulation results and analyzes the effect of the various system parameters. Finally, the paper is concluded in Section VI.

II. Related Work

Most existing underwater localization methods are based on acoustics since it is the standard of communication in water [2][9]. Yet, such a mode of communication is limited to small frequency bands and suffers high attenuation [10]. Meanwhile, VLC provides much higher bandwidth and much better cross-medium performance than acoustics [11]. Recent studies have explored different aspects of VLC communication like channel modeling [12] and achievable performance [13]. However, these studies consider only the water medium. VLC is deemed a viable option for cross-medium communication [6]. Multiple studies have also analyzed the behavior of optics in different water types [14]. In [15], we have leveraged these studies and proposed a method of localizing stationary underwater nodes using the intensity of transmitted light.

GAULA is focused on providing accurate global localization of a dynamic AUV using VLC without deploying anchors on the water surface. Aside from acoustic methods [16], an AUV can also be localized via visual methods [17-18]. But all these methods either perform localization locally or globally using a beacon or anchor on the water surface, which sometimes can be detrimental to the application. GAULA overcomes these limitations and provides global localization to an AUV without the involvement of a physical anchor.

III. SYSTEM MODEL AND BACKGROUND

A. System Model and Assumptions

GAULA is geared for applications where one or multiple AUVs are deployed in an area of interest. Without loss of generality, such an area is assumed to be square-shaped. The AUV moves unconstrained in the area along the x, y and z-axis. The AUV has: (1) a navigation system to track its trajectory, (2) pressure sensor to measure its underwater depth, and (3) a VLC receiver. We consider the water surface as the *x-y* plane, and the water depth as the *z*-axis. An airborne node (AN) is employed to assist the AUVs in localizing themselves. The AN could also perform other duties, e.g., providing commands to the AUVs; yet we

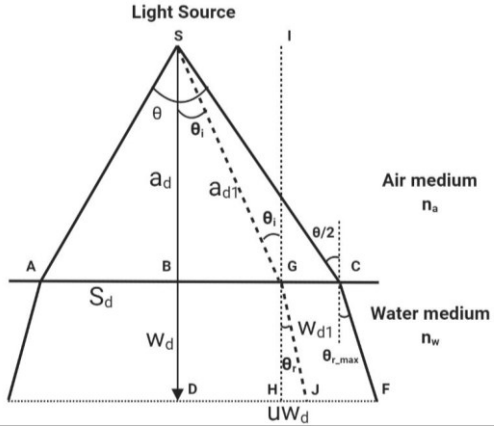


Fig. 2: A 2D illustration of the coverage of light transmission from a source at *S* above the water surface.

focus only the AN role in the localization process. The AN is assumed to be equipped with a GPS and a VLC transmitter. Periodically, the AN scans the area and transmits VLC beams, per the GAULA protocol. The AN is assumed to move at a constant speed.

B. Light Intensity Measurement and VLC-Ranging

Islam et al. [6] have analyzed how the coverage area of a light beam underwater and shown the correlation of the light intensity with proximity to the incident point. For a uniform light source, the underwater coverage will be circular, and the intensity of light at a certain depth is constant for the same distance from the beam incident point. In Fig. 2, the light intensity at point J is:

$$I = \frac{360}{\theta} \cdot \tau \cdot \frac{P}{4\pi \left(\frac{a_d}{\cos \theta_l}\right)^2} \cdot e^{\frac{-ka_d}{\cos \theta_r}} \tag{1}$$

where the parameters are defined in Table 1. Thus, an AUV can use the measured light intensity to infer how far it is from the incident point in the *x-y* plane (recall an AUV knows its depth).

In [9], we have leveraged such analysis and proposed a method to localize stationary underwater nodes and provide them with global coordinates using multilateration. Our method maps the area into a grid where the AN targets the center of each square-shaped cell with a VLC transmission providing the AN's GPS coordinate and height. Eq. (1) is used to assess proximity to the cell center; by receiving at least three transmissions the underwater node can apply multilateration to calculate its position relative to the grid and uses the known coordinates of the cell center to determine its global coordinates. GAULA opts

Table 1: Definition of the used notation

Notation	Description
P	Power of the light source
θ	Beam angle of the light source for flat surface
$ heta_i$	Incident angle of water surface for flat surface
θ_r	Refraction angle for flat surface
a_d	Distance of light source from water surface for flat surface
w_d	Depth of the sensor from water surface for flat surface
η	Reflectance of light
τ	Transmittance of light

to overcome the limitation of such a method by enabling localization of mobile underwater vehicles.

IV. LOCALIZATION OF UNDERWATER MOBILE NODES

Unlike the case of stationary nodes, localizing an AUV is quite challenging. First, both the AN and AUV move in an uncoordinated manner. While the AN motion pattern can be controlled, the AUV travel path and speed depend on the application, e.g., what event has emerged, what object is being tracked, etc. Second, there is no common reference grid for both the AN and AUV. The grid reflects the area scanned by the AN; yet the AUV does not know where it is located within the grid. Moreover, the transmissions that the AUV receives are not for the same cell and hence spatial correlation of these transmissions is necessary. Such correlation is not straightforward given that the AUV does not know the reference grid. In the balance of this section we explain how GAULA tackles these challenges.

A. Virtual Anchor Points

GUALA exploits the use of AN to make targeted VLC transmissions. The idea is to define points with known coordinates; the points serve as virtual anchors that are uniformly distributed in the area. To do so, the AN overlays a grid of square-shaped cells over the AUV operation area. The size of the cell is subject to a trade-off as we discuss later in this section. The AN hovers over the water surface and traverses the cells in a specific order. The order would normally depend on the travel speed of both the AUV and the AN. For each cell, the AN directs a light beam that is encoded to convoy the GPS coordinates of the AN at that instant of time, which reflects the x and y coordinates of the surface point, while the z-axis reflects the altitude of the AN. The AN also includes the flight speed and necessary parameters such as beam angle, and the transmission power so that the AUV can apply eq. (1).

With respect to the AN, there are three important parameters that affect the success of GAULA, namely, the cell size, cell visiting order, and number of VLC transmissions per cell. A larger cell size would increase the prospective that AUV will receive the transmission; yet growing the cell size requires wider beam angle, increase power losses, and diminish the light intensity underwater [6]. On the other hand, pursuing smaller cells would increase the cell count and consequently the number of anchor nodes. The underwater light intensity will increase as well, allowing the AN to reach AUVs deep in the water. However, fast-moving AUV could pose a challenge in such a case since there is high probability that the AN and AUV will not rendezvous at the same cell, causing the AUV localization process to fail in getting sufficient measurements. Having some knowledge of possible AUV motion patterns and speeds would be beneficial in setting the cell size. The cell visiting order, and number of VLC transmissions per cell would also depend on the difference between the AN and AUV speeds. The effect of AN and AUV speed will be analyzed at the end of this section.

B. AUV Motion Tracking

An AUV is usually equipped with INS to guide its navigation through the water. Dead reckoning is a popular method for tracking trajectory using the gyroscope and accelerometer to measure the linear and angular acceleration of the AUV. Specifically, the vehicle can measure its angles, α , and β , relative to the z-axis (depth) and the x-axis in its own x-y plane,

respectively, and after traveling a distance, d, from its previous position. Thus, if the AUV moves from point (x_1, y_1, z_1) , to point (x_2, y_2, z_2) , we have:

$$z_2 = z_1 + d.\cos\alpha \tag{2}$$

$$x_2 = x_1 + d. (\sin \alpha). (\cos \beta) \tag{3}$$

$$y_2 = y_1 + d.(\sin \alpha).(\sin \beta) \tag{4}$$

In practice, the distance and angle measurements could be subject to errors, d_e , α_e , and β_e . A high-quality INS can achieve a drift of 0.1% [21] and is assumed in our simulation, as discussed in Section IV. The travelled distance is estimated based on the speed and duration. In the rest of this section, we plan to focus on the x-y plane since the AUV knows its depths.

The AUV trajectory is defined by the application needs; therefore, the underwater region covered by an AUV should be bounded and known. An important goal of the global location of GAULA is to prevent the AUV from drifting away and enabling it to stay within the desired region. Generally, the AUV does not know when the AN is deployed and becomes aware only when it receives VLC transmissions. Hence, synchronized AUV and AN motion is not possible. In fact, the number of received VLC transmissions by the AUV depends on the difference between its motion speed and that of the AN, as elaborated later in this section.

C. Global Coordinates Estimation

When making a VLC transmission, the AN includes its GPS and the power of the emitted light beam in the packet. Upon receiving the AN transmission at time t_i , the AUV will be able to determine its proximity to the cell center (beam incident point) using eq. (1). Unlike the stationary underwater node, we must factor in the vector movement while localizing the AUV. If the AUV moves spatially for τ time units with a known vector (speed, time and angle respective to its axes), we can project this circle with that vector and get the possible location of the AUV after τ time units elapsed.

For example in Fig. 3(a), the first transmission is made at time t_l while the AN is at point (x_1, y_1, z_1) . Based on the sensed light intensity, the AUV estimates that it is located at a distance r_1 from the projected incident point in the x-y plane, namely (x_1, y_1) . After τ time units, the AUV receives another transmission, for which the center of the projected circle will be (x_2, y_2) ; the AUV is estimated to be r_2 away from such a center and the distance between the centers of the first and second circles is d. During that time the AUV travels with a known vector direction, Θ_l , and length, d_1 . As seen in Fig. 3 (a), the two circles do not

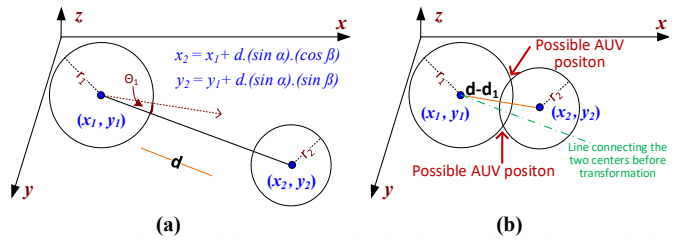


Fig. 3: (a) Projection of the AUV position in the x-y plane. The two circles reflect the range of VLC transmissions at coordinates (x_l, y_l, z_l) and (x_2, y_2, z_2) . The AUV could be at any point on the circumference of the shown circles. (b) The position of the 2^{nd} transmission is transformed to coincide with the 1^{st} transmission, i.e., τ time units earlier. The intersection of circles narrows the set of possible positions that the AUV could be at during the 1^{st} transmission.

intersect and reflects positions of AUV at t_l and $t_2 = t_l + \tau$. By transforming the second location back in time one can narrow the possible positions. For the considered example, the AUV has traveled in straight line for a distance d_l and at an angle θ_l . By rotating the line connecting the two centers for $-\theta_l$, and moving the second circle along the new line for a distance d_1 , i.e., the two centers become $(d-d_1)$ apart, we calibrate the measurements to the same reference coordinate system. As seen in Fig. 3(b), such transformation causes the two circles to intersect at two points, which reflects where the AUV at time t_l .

Generally, the transformation could lead to one, two, or no intersections between the two circles. As we are considering two circles, they cannot intersect at more than two points. If they intersect at only one point, i.e., the circles would have a common tangent, such a point becomes the definite position of the AUV and the global coordinates can be determined. Note that (x_1, y_1) and (x_2, y_2) cannot be the same point given the AN's motion pattern. On the other hand, there is a chance that the two circles do not intersect, which could be caused by errors in the INS measurements, i.e., significant d_e , α_e and β_e . We will address this case later in this subsection. If the intersection is at two points, additional received transmissions are needed so that the AUV can further narrow the choice. Fig. 4 shows the example in Fig. 3(b) after receiving a transmission at point (x_3, y_3, z_3) and applying both projection and transformation.

Finally, if the circles corresponding to the first two transmissions do not intersect we can switch order, i.e., try the second and third circles second and then consider the first. In such a case the same logic discussed earlier and illustrated in Fig. 4 would apply. On the other hand, if all consecutive circles do not intersect, we then need to consider the possible errors, d_e , and β_e , to further adjust the circles so that they intersect. Overall, the accuracy of the calculation could benefit from more transmissions and further consideration of possible INS errors. In such a case, a least square error optimization could be formulated to find the best estimate of the AUV trajectory that fits the information inferred from the VLC transmissions.

D. Effect of Relative Speeds

As mentioned before, the AN is transmitting cell-wise and in sequential manner so that it can cover the whole deployment area since it has no knowledge of the AUV position. In addition to the cell size, there are three additional parameters that significantly affect the performance of GAULA, namely the AUV motion trajectory, the AN's flight path (i.e., cell visiting

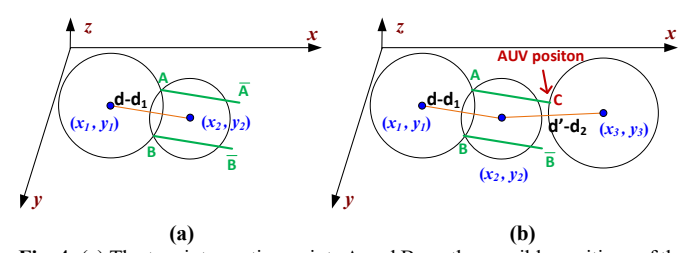


Fig. 4: (a) The two intersection points A and B are the possible positions of the AUV at time t_I , hence at time t_2 the AUV should be at either \bar{A} or \bar{B} , where the lines $A\bar{A}$ or $B\bar{B}$ are parallel to the line connecting (x_1, y_1) and (x_2, y_2) . (b) when a third transmission is received, the AUV repeat process and try to exclude either \bar{A} or \bar{B} , where in this case the line intersects with the third circle and hence the AUV is present at point C.

order), and the relative motion speeds of the AN and AUV. We have discussed the trade-off in setting the cell size in section IV-A. The cell-size setting itself is a function of the motion and speed of the AN and AUV. Similarly, the AUV motion trajectory and the AN's flight pattern will influence the received transmission count for the AUV, consequently the feasibility and accuracy of the localization process. Fundamentally, the area scanning should achieve maximum coverage since the AUV trajectory is unknown; yet the effect on localization also depends on the relative AN and AUV speeds. Hence, we focus on the latter in the balance of this subsection.

AUVs have a typical speed of 1.5-2.0 m/s [19]. A commonly bought quadcopter can achieve a speed of up to 20 m/s. Depending on the model and cost of the AN, this speed can rise up to 30-45 m/s. So typically, the AN is much faster than the AUV. Depending on the speed difference between AN and AUV, the AUV will either receive enough transmission or not. To illustrate let us consider the example in Fig. 5(a), where the AUV is under the coverage of the first three AN's transmissions provided that the AUV had started its journey from the first cell when it received the transmission. If the AN speed is much higher than that of the AUV, by the time the AN gets to the third cell and transmits, the AUV will lag behind and will be out of the range, as shown in Fig. 5(b). Due to the AN flight and AUV motion patterns, the AUV could receive its third transmission at cell #17, and become localizable.

To mitigate the effect of speed difference, we exploit the variability in the beam angle. Generally, the underwater coverage of a VLC transmission depends on several parameters, namely, the emitted power, beam angle, AN height, and AUV depth. Obviously the AUV depth cannot be controlled by the AN. Among the other three parameters. The beam angle is the easiest to control since: (i) it is expected that AN uses the most possible power in order to increase the underwater reach of the VLC transmission, and (ii) changing the AN height is mostly mechanical and would not be fast enough. The idea is for GAULA to vary the beam angle among consecutive cells in order to change the coverage in the x-y plane and along the depth. For example, the AN may alternate between two angles when flying across cells. In addition, pursuing multiple scans is recommended where the cells are visited in different sequences. For example, row-by-row scan could be first conducted and then followed by a diagonal scan. We study the performance of these options through simulation as explained in Section V.

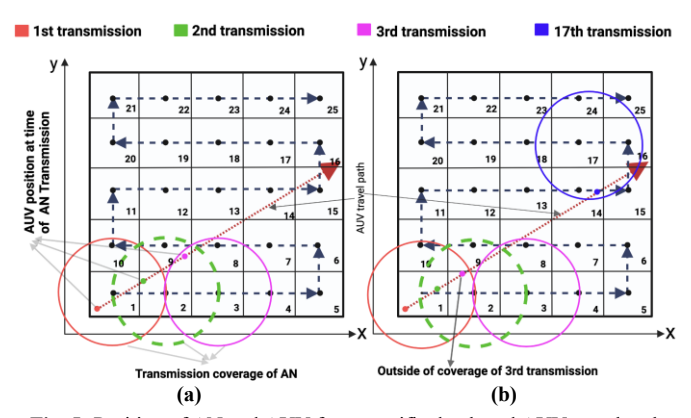


Fig. 5: Position of AN and AUV for a specific depth and AUV travel path for: (a) lower, and (b) higher speed difference of AN and AUV.

E. Localization Error Minimization

As pointed out earlier, the INS measurements are subject to error, which in turn accumulate and diminish the localization accuracy. Generally, d_e , α_e , and β_e vary throughout the AUV trajectory and follow a Gaussian distribution. GAULA further mitigates the impact of accumulative errors by formulating a least square optimization to find the most accurate estimated positions for the AUV that correspond to AN's transmissions. If the AUV travels a distance d_i at angles α_i and β_i relative to the z and x axes when receiving the ith transmission, the error components in the x, y and z directions are dx_i , dy_i and dz_i and the corresponding relative coordinates are:

$$z_{ei} = z_{i-1} + d_i \cdot \cos \alpha_i + dz_i \tag{5}$$

$$x_{ei} = x_{i-1} + d_i. (\sin \alpha_i). (\cos \beta_i) + dx_i$$
 (6)

$$y_{ei} = y_{i-1} + d_i.(\sin \alpha_i).(\sin \beta_i) + dy_i$$
 (7)

Assuming that the AUV receives n transmissions during its journey, the objective function is to minimize:

$$f(d,\alpha,\beta) = \sum_{i=0}^{n} ((x_{ei} - x_i)^2 + (y_{ei} - y_i)^2 + (z_{ei} - z_i)^2$$
 (8)

Such formulation can be solved using the Levenberg-Marquardt algorithm, which works by iteratively updating the values of d, α , and β to reduce f. At each iteration, the algorithm computes the gradient and Hessian of $f(d, \alpha, \beta)$, and uses them to determine the direction and step size of the update.

V. PERFORMANCE VALIDATION

A. Simulation Environment

GAULA is validated through simulation using MATLAB. The AN has a beam angle of 60°, flies at a height of 5 meters from the surface of the water, and is equipped with a transmitter that has enough power to achieve the required light intensity at the preferred depth. Some parameters are subjected to variation due to instrumentation and measurement errors. These fluctuations can be represented as white Gaussian noise and contribute to

parameters such as power, AN height measurement, and depth measurement pressure sensor reading. These errors will affect the intensity calculation in eq. (1) and, consequently, the distance measurement. Generally, these errors can be reduced by using high-quality well calibrated sensors. Yet, the INS is the significant cause of errors in GAULA, specifically, affecting equations (2) – (4). The effect of INS errors further accumulates over the distance the AUV is traveling. In the simulation, we consider spatial and angular displacement errors with Gaussian distribution with zero mean and a standard deviation of 1%, i.e., values of d_e , α_e , and β_e . The water quality is considered pure sea water which has an attenuation coefficient of 0.056.

B. Simulation Results

To study the effect of various parameters on the localization performance, we have considered a deployment area of 25×25 meters that is mapped to a 25-cell grid. The travel path of the AN is as shown in Figure 5. We assume that the AUV starts at the first cell (bottom left corner) where it receives its first VLC transmission. The AUV cuts across the area at a fixed angle, ϕ . relative to the x-axis and at constant speed. Such an angle and the difference between the AN and AUV speeds, Δ , are varied across experiments. Table 2 compares the number of received transmissions and the corresponding localization error (in meter) at 2-meter depth for various Δ and ϕ values. The table indicates that localizability, i.e., getting at least three transmissions, improves with the growth of ϕ ; yet the speed difference is very influential. If both the AUV and AN travel at the same speed (i.e., Δ =0), a high value of ϕ implies that the AUV will visit fewer cells and hence the probability that the AN and UAV trajectories overlap diminishes. Similar rationale applies as ϕ gets close to 90°. As the AN speed becomes more dominant, e.g., exceeding the AUV speed by more than 10 m/s, the probability of catching the AUV diminishes and too few transmissions become available for localization

Speed difference	0 m/s		0 m/s 2 m/s		4 m/s		6 m/s		8 m/s		10 m/s		17.5 m/s		27 m/s	
ф	Contact	Error	Contact	Error	Contact	Error	Contact	Error	Contact	Error	Contact	Error	Contact	Error	Contact	Error
0°	5	UL	1	UL	1	UL	1	UL	1	UL	1	UL	1	UL	1	UL
10°	5	0.156	1	UL	1	UL	1	UL	1	UL	1	UL	1	UL	1	UL
20°	4	0.162	2	UL	1	UL	1	UL								
30°	2	UL	2	UL	3	0.193	2	UL	1	UL	1	UL	1	UL	1	UL
40°	2	UL	2	UL	6	0.147	2	UL	2	UL	1	UL	1	UL	1	UL
50°	1	UL	1	UL	7	0.159	3	0.137	3	0.113	2	UL	1	UL	1	UL
60°	1	UL	1	UL	4	0.167	6	0.112	2	UL	2	UL	1	UL	1	UL

Table 2: Localization accuracy for various speed differences at 2-meter depth (25 Cells).

Table 3: GAULA performance for various speed differences at 2-meter depth (100 cells).

Speed difference	0 m/s		2 m/s		4 m/s		6 m/s		8 m/s		10 m/s		20 m/s		70 m/s	
ф	Contact	Error														
0°	11	0.061	4	0.045	3	0.11	3	0.114	3	0.126	3	0.078	3	0.059	3	0.031
10°	11	0.074	5	0.046	7	0.104	4	0.116	4	0.117	4	0.075	4	0.058	3	0.046
20°	5	0.077	4	0.134	10	0.091	11	0.086	8	0.099	7	0.068	4	0.061	3	0.039
30°	4	0.091	2	UL	8	0.099	14	0.085	17	0.078	10	0.061	5	0.055	4	0.043
40°	3	0.095	2	UL	2	UL	9	0.104	24	0.079	22	0.059	5	0.056	4	0.049
50°	2	UL	2	UL	2	UL	5	0.134	15	0.091	29	0.058	8	0.055	4	0.037
60°	2	UL	2	UL	2	UL	2	UL	7	0.104	21	0.062	9	0.053	4	0.044
70°	2	UL	2	UL	2	UL	2	UL	6	0.132	12	0.059	8	0.056	3	0.037
80°	2	UL	2	UL	2	UL	2	UL	4	0.144	8	0.068	10	0.054	3	0.039
90°	2	UL	2	UL	2	UL	2	UL	3	0.146	6	0.079	8	0.062	3	0.046

consequently the error grows or the AUV even becomes non-localizable.

To capture the effect of underwater depth, we have repeated the simulation of Table 2, while having the AUV at 5-meter depth. We have observed a slight increase in received transmissions and about 10-15% reduction in localization error compared to Table 2. Such performance improvement is mainly attributed to the growth in coverage (see Fig. 2), which boosts the probability for the AUV to receive multiple transmissions. Nonetheless, as Δ exceeds 10 m/s the effect of coverage seizes for this configuration. Table 3 shows the GAULA performance at 2-meter depth in the same deployment area; yet a grid of 100 cells is used instead. In addition to the improved performance in terms of the number of received transmissions and the associated localization error, compared to Table 2, we observe greater speed tolerance in this case. Even at the speed difference of 70 meters per second, the AUV could still be localized. We also note that the localization error diminishes as the speed difference between the AN and AUV increases. This is attributed to the fact that most received transmissions are in the same and closeby cells and hence the effect of INS errors becomes insignificant.

Fig. 6(a) captures the effect of varying beam angles on the localization performance of GAULA where the AN's height is 5 meters, and the AUV is at depth of 2 meters, and the area is mapped to a grid of 25 cells. The reported results represent the average error when the node first becomes localizable for varying relative travel angles. The transmission pattern of the AN is the same as in Fig. 5, assuming that the AUV begins its journey at the first cell. The results indicate that with a wider beam angle the node becomes localizable quicker, hence less INS error gets accumulated. Yet, the wider beam angle necessitates a higher VLC transmission power for the AN to reach the AUV. Fig. 6(b) studies the impact of the area scanning pattern on localization error. The first pattern is shown in Fig. 5, while the second is of diagonal nature following the sequence cell 1, (cell 2, 10), (cell 11, 9, 3), (cell 4, 8, 12, 20) and so on. The beam angle is set to 60° and the setting of other parameters stays the same as Fig. 6(a). The results show that the scanning pattern is not that influential, which is expected given that the AN and AUV are not coordinating. As shown below their relative travel speeds significantly affect the localization error.

VI. CONCLUSION

This paper has presented, GAULA, a novel approach to globally localize an AUV using an airborne node. The idea is based on directing modulated VLC transmissions from the air to certain positions on the water surface. The VLC transmission includes the GPS coordinates and height of the AN. The light

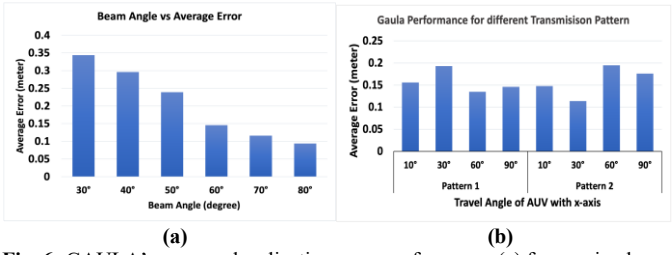


Fig. 6: GAULA's average localization error performance (a) for varying beam angle (b) for different transmission patterns.

penetrates the surface and reaches the underwater node, with intensity that depends on the depth. By having a pressure sensor to determine its depth, an AUV uses the light intensity of the received AN transmission along with AN position information to define the circumference of a circle that it may be located on. By receiving at least three transmissions and factoring in movement trajectories, the AUV can determine its global coordinates. The simulation results have confirmed the effectiveness of GAULA and provided guidelines on the setting of the influential parameters to minimize the localization error.

<u>Acknowledgment:</u> This work is supported by the National Science Foundation, USA, Contract #0000010465.

REFERENCE

- [1] M. Jouhari, K. Ibrahimi, H. Tembine and J. Ben-Othman, "Underwater Wireless Sensor Networks: A Survey on Enabling Technologies, Localization Protocols, and Internet of Underwater Things," *IEEE Access*, vol. 7, pp. 96879-96899, 2019.
- [2] I. Ullah, J. Chen, X. Su, C. Esposito and C. Choi, "Localization and Detection of Targets in Underwater Wireless Sensor Using Distance and Angle Based Algorithms," *IEEE Access*, vol. 7, pp. 45693-45704, 2019.
- [3] M. Mahmud, M. S. Islam, A. Ahmed, M. Younis, F.-S. Choa, "Cross-Medium Photoacoustic Communications: Challenges, and State of the Art," Sensors, 22(11), pp. 4224, 2022.
- [4] M. V. Jamali, A. Chizari, and J. A. Salehi, "Performance Analysis of Multi-Hop Underwater Wireless Optical Communication Systems," *IEEE Photonics Technology Letters*, 29(5), pp. 462-465, March 2017.
- [5] H. Kaushal and G. Kaddoum, "Underwater Optical Wireless Communication," *IEEE Access*, vol. 4, pp. 1518-1547, 2016.
- [6] M. S. Islam and M. F. Younis, "Analyzing Visible Light Communication Through Air–Water Interface," *IEEE Acc.*, 7, pp. 123830-123845, 2019.
- [7] M. S. Islam and M. Younis, "An Adaptive DPPM for Efficient and Robust Visible Light Communication Across the Air-Water Interface," Proc. of the 29th Wireless and Optical Comm. Conf. (WOCC), Newark, NJ, 2020.
- [8] M. S. Islam, M. Younis, M. Mahmud and J. B. Saif, "A Novel Encoding Scheme for Improving the Bandwidth Efficiency of DPPM," Proc. IEEE International Conference on Communications (ICC), 2021, pp. 1-6.
- [9] J. Yan, D. Guo, X. Luo and X. Guan, "AUV-Aided Localization for Underwater Acoustic Sensor Networks with Current Field Estimation," *IEEE Trans. on Vehicular Tech.*, 69(8), pp. 8855-8870, Aug. 2020
- [10] N. Li, J.-F. Martínez, J. Meneses Chaus, and M. Eckert, "A Survey on Underwater Acoustic Sensor Network Routing Protocols," *Sensors*, 16(3), p. 414, Mar. 2016.
- [11] C. Shen et al., "20-meter underwater wireless optical communication link with 1.5 Gbps data rate," Opt. Express, 24(22), pp. 25502–25509, 2016.
- [12] F. Miramirkhani and M. Uysal, "Visible Light Communication Channel Modeling for Underwater Environments with Blocking and Shadowing," *IEEE Access*, vol. 6, pp. 1082-1090, 2018,
- [13] M. Elamassie, F. Miramirkhani and M. Uysal, "Performance Characterization of Underwater Visible Light Communication," *IEEE Transactions on Communications*, 67(1), pp. 543-552, Jan. 2019,
- [14] P. Saxena and M. R. Bhatnagar, "A Simplified Form of Beam Spread Function in Underwater Wireless Optical Communication and its Applications," *IEEE Access*, vol. 7, pp. 105298-105313, 2019.
- [15] J. B. Saif and M. Younis, "Underwater Localization using Airborne Visible Light Communication Links," Proc. IEEE Global Communications Conference (GLOBECOM), 2021, pp. 01-06.
- [16] T. Zhang, Z. Wang, Y. Li, and J. Tong, "A Passive Acoustic Positioning Algorithm Based on Virtual Long Baseline Matrix Window," *The Journal of Navigation*, 72(1), pp. 193–206, 2019.
- [17] Y. Wang, X. Ma, J. Wang and H. Wang, "Pseudo-3D Vision-Inertia Based Underwater Self-Localization for AUVs," *IEEE Transactions on Vehicular Technology*, 69(7), pp. 7895-7907, July 2020.
- [18] Jung, J., Li, JH., Choi, HT. et al. "Localization of AUVs using visual information of underwater structures and artificial landmarks," *Intel Serv Robotics*, vol. 10, pp. 67–76, 2017.
- [19] R. B. Wynn, et al., "Autonomous Underwater Vehicles (AUVs): Their past, present and future contributions to the advancement of marine geoscience", *Marine Geology*, vol. 352, 2014, pp. 451-468.